

Article

An Experimental Evaluation of Electron Beam Welded Thixoformed 7075 Aluminum Alloy Plate Material

Ava Azadi Chegeni and Platon Kapranos *

Department of Materials Science & Engineering, University of Sheffield, Sir Robert Hadfield Building, Mappin Street, South Yorkshire, Sheffield S1 3JD, UK; avaazadi.922@gmail.com

* Correspondence: p.kapranos@sheffield.ac.uk; Tel.: +44-114-22-25509

Received: 8 November 2017; Accepted: 13 December 2017; Published: 15 December 2017

Abstract: Two plates of thixoformed 7075 aluminum alloy were joined using Electron Beam Welding (EBW). A post-welding-heat treatment (PWHT) was performed within the semi-solid temperature range of this alloy at three temperatures, 610, 617 and 628 °C, for 3 min. The microstructural evolution and mechanical properties of EB welded plates, as well as the heat-treated specimens, were investigated in the Base Metal (BM), Heat Affected Zone (HAZ), and Fusion Zone (FZ), using optical microscopy, Scanning Electron Microscopy (SEM), EDX (Energy Dispersive X-ray Analysis), and Vickers hardness test. Results indicated that after EBW, the grain size substantially decreased from 67 µm in both BM and HAZ to 7 µm in the FZ, and a hardness increment was observed in the FZ as compared to the BM and HAZ. Furthermore, the PWHT led to grain coarsening throughout the material, along with a further increase in hardness in the FZ.

Keywords: 7075 aluminum alloy; thixoforming; post-welding-heat treatment; electron beam welding (EBW)

1. Introduction

7075 wrought aluminium alloys are used for a wide variety of applications in aerospace and automotive industries due to the outstanding characteristics that they possess, such as high-strength-to-weight ratio, ductility, toughness, low density, and resistance to fatigue [1–4]. Promising fabrication techniques are required to produce high quality and integrity parts for such applications. Hence, semi-solid metal processing as a single step manufacturing method providing good quality near net shape products has been widely employed to aluminium alloys due to the advantages that this technology offers over the conventional casting techniques [5–8].

Weldability of the materials is another important factor in aerospace and automotive industries. However, although Al alloys have in the past been considered as difficult-to-weld materials through conventional arc welding techniques, improvements have removed these difficulties and quite few studies have focused on other technologies that offer improvements of weld performance, such as high-power density fusion joining, namely, laser beam welding (LBW) and electron beam welding [1,9,10], and, of course, Friction Welding.

Electron-beam welding (EBW) is a fusion welding process, in which a beam of high-velocity electrons is applied to two materials to be joined. The workpieces melt and flow together as the kinetic energy of the electrons is transformed into heat upon impact. EBW is often performed under vacuum conditions to prevent dissipation of the electron beam. Electron beam welding provides high-quality welded joints for a wide range of thicknesses, and can be operated with high welding speeds [11,12]. Using EBW generates low distortions in the Fusion Zone (FZ), together with a narrow Heat Affected Zone (HAZ), and low residual stresses in comparison with conventional welding techniques [12,13]. To take advantage of these features, many studies centred around the investigation of the EBW on different aluminium alloys. Cam et al. [14] investigated the effects of EBW on

mechanical properties and microstructural characterisation of 5005, 2024, and 6061 aluminium alloys, and concluded that a defect free weld line was observed in these alloys. Kocak et al. [12] also evaluated the impacts of EBW on aluminium 7020 alloy, and reported that a loss of hardness in FZ was observed due to the loss of strengthening phases. Currently, there is no reported data published on EBW of thixoformed aluminium 7075 alloy and the aim of this study is to investigate the effect of EBW on the microstructure and mechanical properties of two thixoformed aluminium plates of Al 7075 alloy. These results have been obtained through optical microscopy, Scanning Electron Microscopy (SEM), EDX (Energy Dispersive X-ray Analysis) on the electron beam welded plates, along with hardness measurements. In addition, a post welding heat treatment of the weld zone was conducted at the semi-solid temperature range in order to investigate any microstructural and property changes in the weld material, as well as the parent material. The choice of the Semi-solid range was to replicate the conditions experienced during the thixoforming process that takes place within this temperature range at approximately 50% liquid content.

2. Materials and Methods

Two thixoformed plates of 7075 wrought aluminium alloy were used as starting materials. The chemical composition of the alloy is presented in Table 1 [1].

Table 1. Chemical composition of wrought 7075 Al alloy (wt %) [1].

| Alloy | Cu | Zn | Mg | Mn | Cr | Ti | Si | Fe | Zr | B | Al |
|-------|------|------|------|-------|------|------|------|-------|-------|-------|------|
| 7075 | 0.94 | 4.52 | 2.24 | <0.01 | 0.22 | 0.05 | 0.02 | <0.01 | <0.01 | <0.01 | Bal. |

The plates were welded using electron beam welding with a speed of 1000 mm/min at TWI Ltd. Cambridge (Great Abington, Cambridge, UK). The accelerating voltage and beam current that were used were 130 kV and 21 mA, respectively. The microstructure of the welded plates was investigated using standard optical metallographic methods. Samples that were cut along the length of the weld line and from the parent material were ground with standard SiC grinding paper and polished with 6 and 1 μm monocrystalline diamond suspension and 0.05 μm silica suspension; the specimens were subsequently etched using sodium hydroxide (10 g NaOH diluted with 100 mL water). The microstructures of the Base Metal (BM), HAZ, and FZ were evaluated using a Nikon Eclipse LV150 optical microscope (Nikon, Tokyo, Japan) and TM3030Plus Tabletop Scanning Electron Microscope (Hitachi, Tokyo, Japan). The chemical analysis of the phases was performed using EDX (Energy Dispersive X-ray Analysis, Hitachi, Tokyo, Japan). Image J software (An open platform for scientific image analysis, <https://imagej.net/Welcome>) was used to measure the average grain size from optical images using the linear intercept method, the shape factor of the solid grains, calculated based on their perimeter and area, as well as the liquid fraction content of the specimens. The Vickers hardness measurements were conducted using a Zwick hardness tester (ZHU250CL, Ulm, Germany) with 10 kgf applied force for 10 s across different locations on the plates, as shown in Figure 1, and the average values were reported. To investigate the influence of post welding heat treatment on the microstructure and mechanical properties of the welded plates, specimens were heat treated by being kept for 3 min at 610, 617, and 628 °C, respectively (i.e., within the semi-solid temperature range of the alloy) and fast cooled in water.

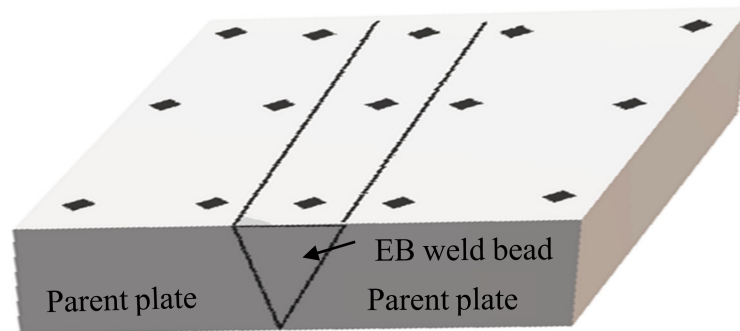


Figure 1. Illustration of the welded plates and the areas of hardness tests.

3. Results and Discussion

3.1. Microstructure of the Base Material

Micrographs of the as-received plate of 7075 thixoformed aluminum alloy are presented in Figure 2; the images are taken from different regions of two plates. When considering Figure 2 from the top left to the bottom right, the microstructure of the alloy is uniform throughout the thixoformed plates, and consists of globular, fine, non-dendritic grains in a solid matrix consisting of the last liquid to solidify.

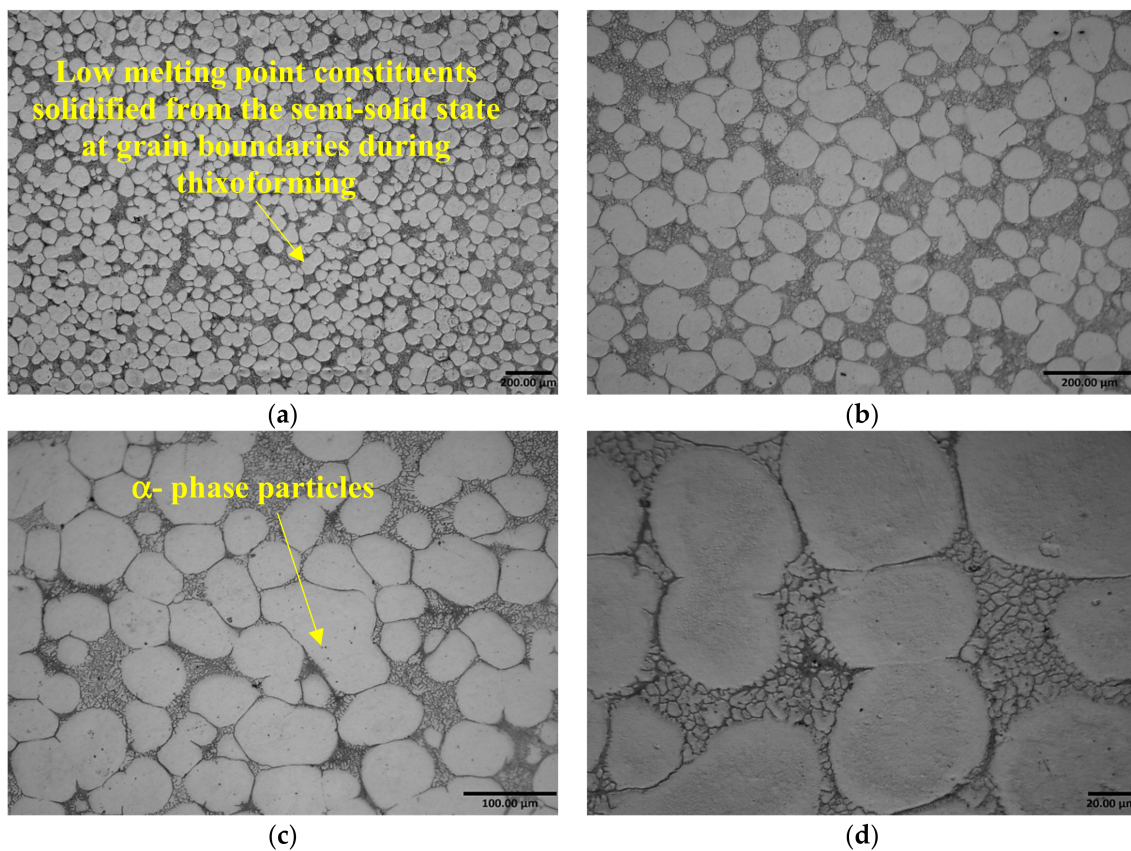


Figure 2. Optical micrographs showing the thixoformed base metal (BM) of 7075 Al Electron Beam (EB) welded plates (a–d) with typical near spheroidal microstructure at different magnifications.

Scanning Electron Microscopy (SEM) micrographs of the BM are shown in Figure 3a,b. It can be observed that the liquid phase specified with a square was formed at the grain boundaries during the thixoforming process. In addition, the last liquid to solidify from the semi-solid state around the grains is illustrated in Figure 3c. There are two ways by which the liquid can be entrapped inside the grains. First, by segregation of the alloying elements inside the solid grains, leading to the formation of fine liquid droplets during the partial re-melting, and, secondly, when grains are combined to reduce the solid-liquid interfacial energy during the heating stage of the thixoforming process, giving rise to the creation of relatively large liquid droplets contained within the sub-grains. Hence, the base metal consists of alpha-Al, eutectic liquid phase and occasional trapped liquid pools within sub-grains [5].

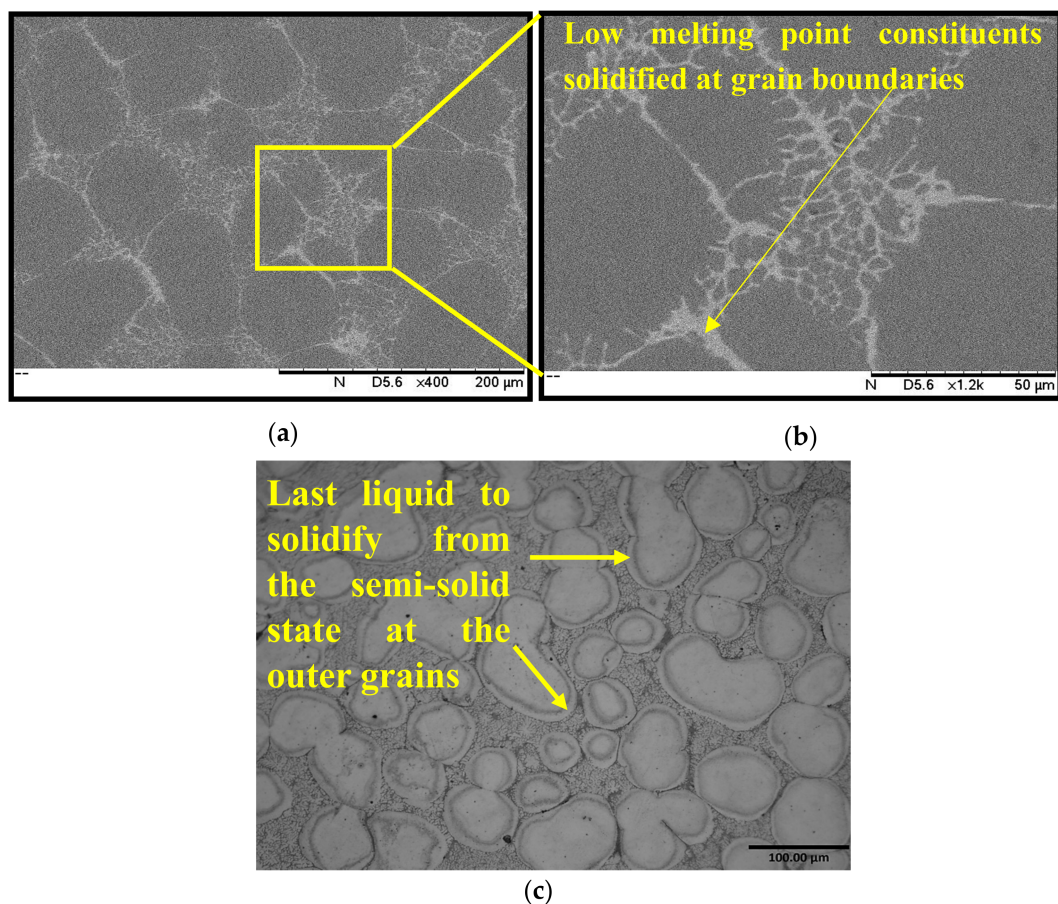


Figure 3. (a) Scanning Electron Microscopy image of Al 7075 alloy showing the last liquid phase to solidify at grain boundaries; (b) a higher magnification SEM image of the liquid phase; (c) optical microscopy image showing the last liquid solidified around the grains.

3.2. Microstructural Evolution after Welding

Figure 4 illustrates the micrographs of the EB welded plates. As can be seen, the microstructure contains three regions, namely, Heat-Affected Zone (HAZ), Fusion Zone (FZ), and Base Metal (BM), as presented in Figure 4a. Generally, high heat input and preheating are two factors that increase the width of the HAZ in precipitation hardenable aluminum alloys. However, it can be observed that the HAZ is relatively narrow due to the low heat input during the electron beam welding process [9,14,15]. In addition, it can be said that although aluminum 7075 alloy is prone to cracking, the EBW process did not pose any significant problems, and only few numbers of pores were formed in the FZ, as shown in Figure 4b. Possible reasons for the formation of these pores could be the high

specific energy density and evaporation of metal that is associated with EBW and thermophysical features of aluminum, including its low melting point, high thermal conductivity, and surface oxide films, with high melting points [9,14,16]. Figure 4c,d show the weld area at different magnifications. As can be observed, the fusion zone consists of a fine grain microstructure with a significant reduction in the average grain size, as compared to the BM and HAZ. As the total heat input into the material during the EBW is lower than that of other fusion welding techniques due to the higher power density of the EBW process, a finer microstructure in the FZ can be typically obtained using EBW. The difference between the grain size in FZ and HAZ is presented in Figure 4e.

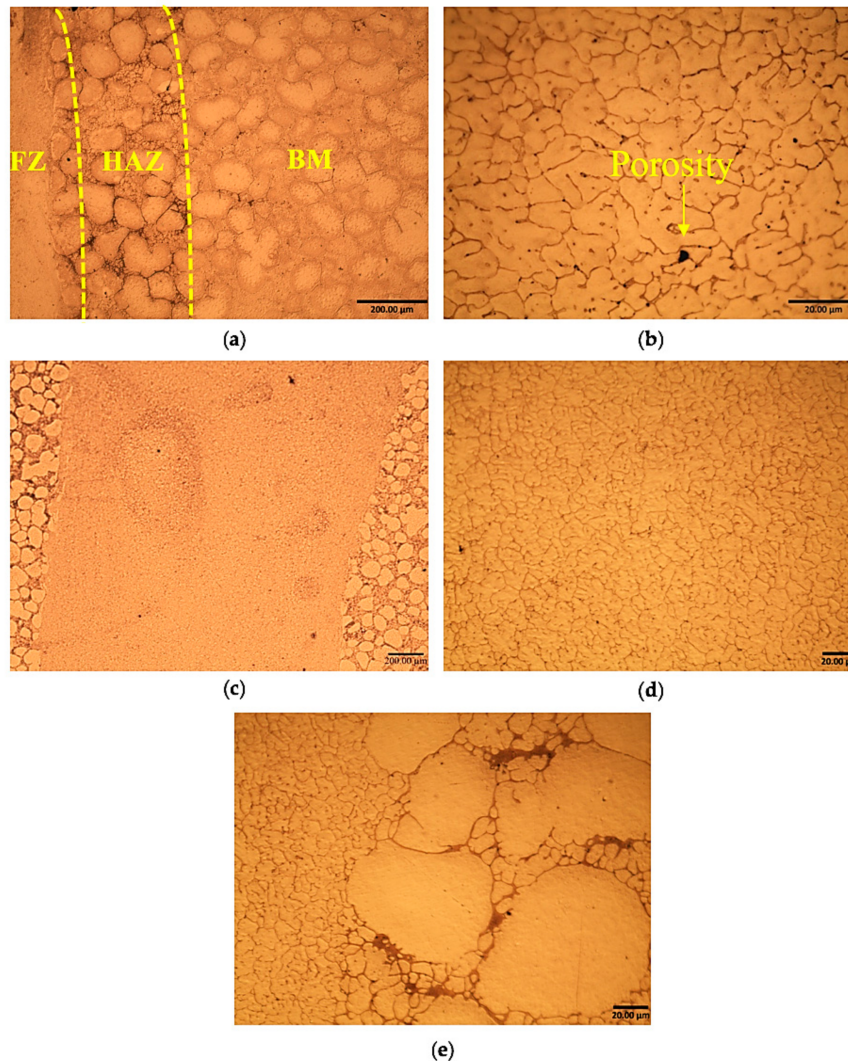


Figure 4. (a) Optical micrographs of Al 7075 EB welded plates, (b–d) show details of the Fusion Zone (FZ) and (e) detail of the plate weld boundary.

Figure 5a shows graphically the grain size as a function of the position from the weld zone. It can be seen that the mean grain size in the BM is around $67\ \mu\text{m}$, and this number is approximately the same in the HAZ, which shows a consistency of the microstructure in the thixoformed plate. However, the grain size in the FZ is significantly reduced to around $7\ \mu\text{m}$, which is considerably smaller than that of either the BM or HAZ. There are several reasons for the reduction of the grain size after welding. First, the presence of the alloying elements that precipitated out at the grain boundaries impedes the severe growth of the grains. In addition, the fast cooling of the joint after the welding process can also prevent grain growth in the FZ [17]. Furthermore, due to the high welding rates of the EB

process that are caused by the high melting speeds of the focused heat source, the time that is required for the welding to be accomplished is also reduced so that the grains do not have enough time to grow during the EBW [12]. Figure 5b demonstrates a graph of the shape factor against the distance from the weld area. The shape factor represents the circularity of the grains, which has a maximum of one for a totally spherical grain and zero for a grain with a complex shape. As can be seen from the graph, more spherical grains can be observed in the BM when compared to the HAZ and FZ, since the material was exposed to the high temperatures during the EBW, leading to the deviation from the spherical grains that are present in the BM. Measurements were taken across various positions in the different zones, and there is clearly a deviation between the spheroidicity of the different grains, as expected as the FZ has undergone melting that destroyed the original non-dendritic, near spheroidal microstructure of the base material.

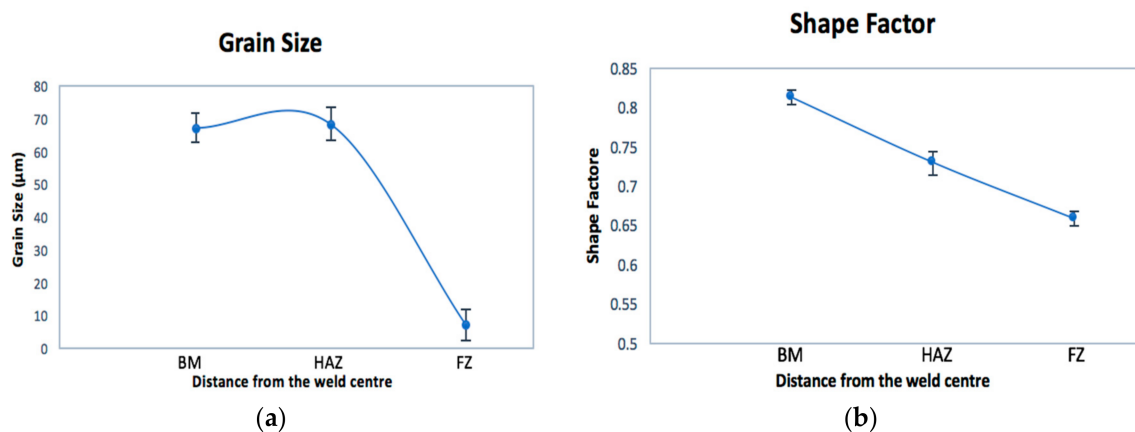


Figure 5. (a) Graph of grain size as a function of position, (b) Graph of shape factor against position.

Results of the EDX point analysis conducted for the last liquid to solidify phase at the boundaries and grains in the BM, as well as the grains in the FZ are shown in Figure 6 and Table 2. From the graphs, it can be said that the liquid phase at the boundaries mainly consisted of aluminum, magnesium, copper, and zinc, implying the presence of the alloying elements in these regions. In addition, it can be observed that aluminum was by far the highest constituent of the grains in the base metal, whilst the percentage of the other elements was low within the grains, which confirms that the alloying elements precipitated out at the boundaries. Moreover, aluminum is the main element in the FZ, with almost the same content as that of the BM. However, EDX point analysis reveals that the matrix phase in FZ contains less Zn than the BM matrix, whereas the Mg and Cu contents of the FZ are higher than that of the BM. Cam et al. [9] suggested that the heat input during the fusion welding processes may give rise to the evaporation of the solute atoms with low melting points in the fusion zone, hence, the lower amount of zinc in this region can be attributed to the evaporation mechanism due to the high amounts of heat applied during welding. The loss of Mg/Zn/Cu was also reported by other researchers [12,14]. Furthermore, rapid cooling after the EBW process leads to the presence of super saturated amount of Mg and Cu in the FZ. It is worth adding that the EDX data for the liquid phase at the boundaries in the FZ could not be measured due to the low amount of the last liquid to solidify phase that remained at the boundaries after EBW.

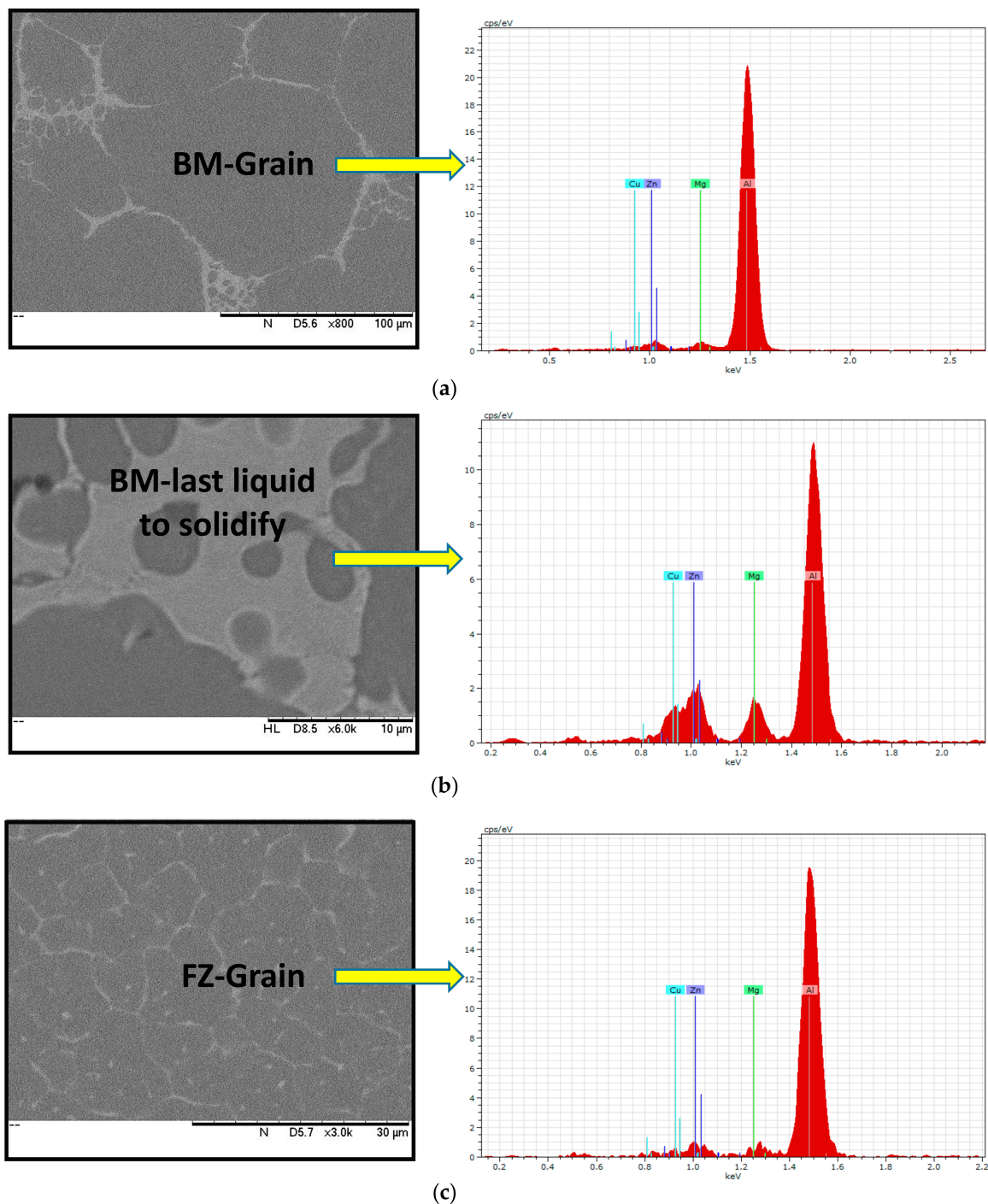


Figure 6. Results of Energy Dispersive X-ray Analysis (EDX) point analysis for: (a) grains in BM, (b) eutectic phase at boundaries, (c) grains in FZ.

Table 2. Weight percent of alloying elements at different points of microstructure. Reported numbers are the average of at least three attempts.

| Locations | Al (wt %) | Zn (wt %) | Mg (wt %) | Cu (wt %) |
|-------------|-----------|-----------|-----------|-----------|
| BM-Grain | 92.2825 | 4.5225 | 2.242 | 0.94075 |
| BM-Boundary | 65.91 | 15.453 | 10.39 | 8.216 |
| FZ-Grain | 91.105 | 4.2145 | 2.65 | 2.018 |

The amount of the last liquid to solidify phase on quenching was calculated using image J software, and a plot of liquid fraction versus distance from the weld centre is indicated in Figure 7. The graph represents a downward trend from the BM to FZ, which suggests that the fraction of eutectic, which is around 35% in the thixoformed plate, is higher than this amount in both HAZ and FZ, which is 22% and 16%, respectively. The higher percentage of the eutectic phase in the BM can be related to the nature of the semi solid metal processing technique, which typically contains between 30–50% liquid. On the other hand, the lower amount of the eutectic phase in the FZ can be attributed to the complete melting in the FZ during the EBW, followed by the fast cooling of this region. It is worth pointing out that the actual amount of the eutectic phase in the BM is higher than the above mentioned number, as can be seen from the micrographs, since some of the liquid is entrapped within the grains and the software could not measure it during the calculations. We will use the terms eutectic solid and last liquid to solidify interchangeably as the terminology used in the Semi-solid forming usually refers to the eutectic solid as liquid fraction.

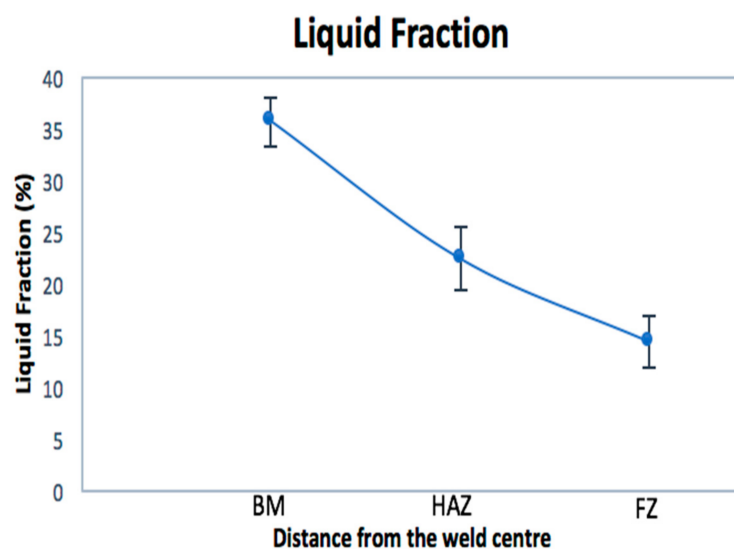


Figure 7. Liquid fraction against distance from the centre of the weld for Al 7075 alloy EB welded plate.

3.3. Post Weld Heat Treatment

Micrographs of EB welded specimens following heat treatment at 610, 617, and 628 °C are presented in Figure 8. According to Figure 8a, the microstructure of the base metal and the heat affected zone at different temperatures consisted of fine equiaxed solid grains that are uniformly distributed throughout the material; which is similar to that of the welded material before the heat treatment. The differences between the grain size of the FZ and HAZ can be observed from Figure 8b. Micrographs of the fusion zone for heat-treated samples, at the three temperatures, are displayed in Figure 8c, as compared to the microstructure of the joint before the post weld process. The grain structure in the FZ has coarsened after heat treatment at three temperatures. In addition, there is a noticeable change in the morphology in this region, in that grains are more spherical in the FZ when compared to the as-received grain structure. This can be explained due to the post weld heat treatment in the semi-solid temperature range to which the material was subjected.

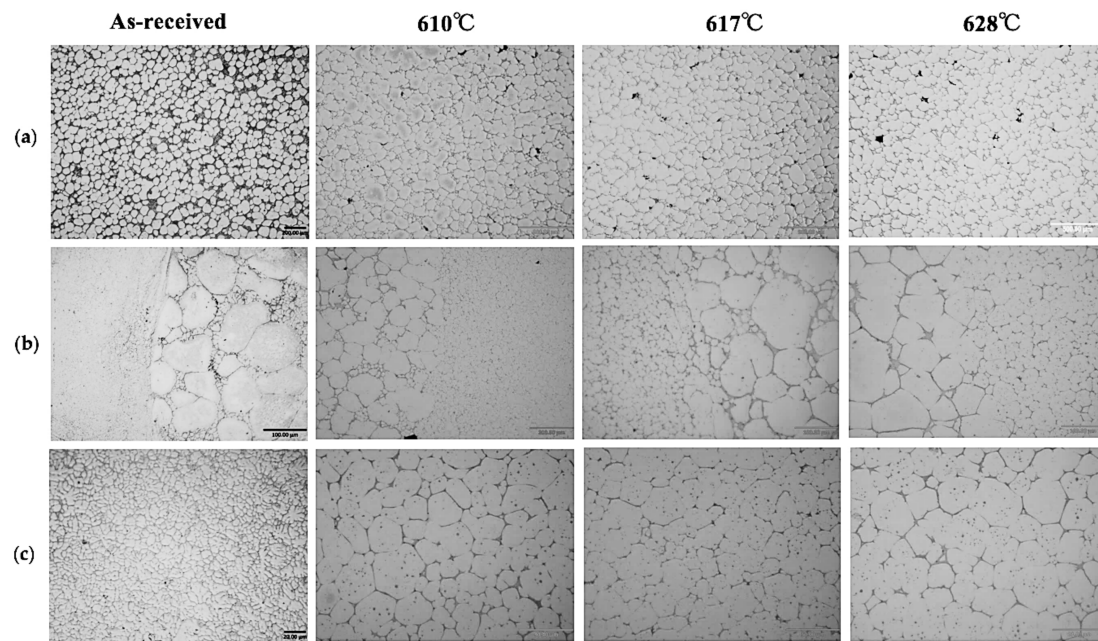


Figure 8. Optical microscopy micrographs of Al 7075 alloy EB welded plates after heat treatment at three temperatures: 610, 617 and 628 °C. (a) as received plate material, (b) HAZ and plate boundary and (c) FZ weld area. (Magnifications top from left to right in μm : 200, 500, 500, 500); (magnifications middle from left to right in μm : 100, 200, 100, 100); (magnifications bottom from left to right in μm : 20, 50, 50, 50).

A graph representing the grain size of the BM, HAZ, and FZ for the heat-treated materials at 610, 617, and 628 °C is shown in Figure 9a. From the graph, it can be seen that the mean grain size in the BM, HAZ, and FZ follows a similar trend, with a slight reduction in the grain diameter at 617 °C, followed by a rise in the average grain size at 628 °C. It is worth adding that grains started to grow in all three regions of specimens, including BM, HAZ, and FZ when compared to the grain structure before the heat treatment. This is due to the exposure of samples to high temperatures during the heat treatment and holding at these temperatures for three minutes, resulting in the grain coarsening. Moreover, the average grain size in the BM is slightly higher than that of the HAZ, but the mean grain diameter in the FZ is by far lower than those in both HAZ and BM, as shown in the micrographs of Figure 8b. Figure 9b shows the shape factor measurement for the heat-treated specimens. As can be seen, there is a significant change in the shape factor of particles in the FZ when compared to before heat treatment. During the heat treatment, solid grains in the FZ became more spherical as they were heated up to the thixoforming temperature range and held for three minutes at these temperatures. The shape factor of grains in the HAZ at the three temperatures is almost the same. In addition, the circularity of the particles in the BM has experienced an upward trend with temperature increase.

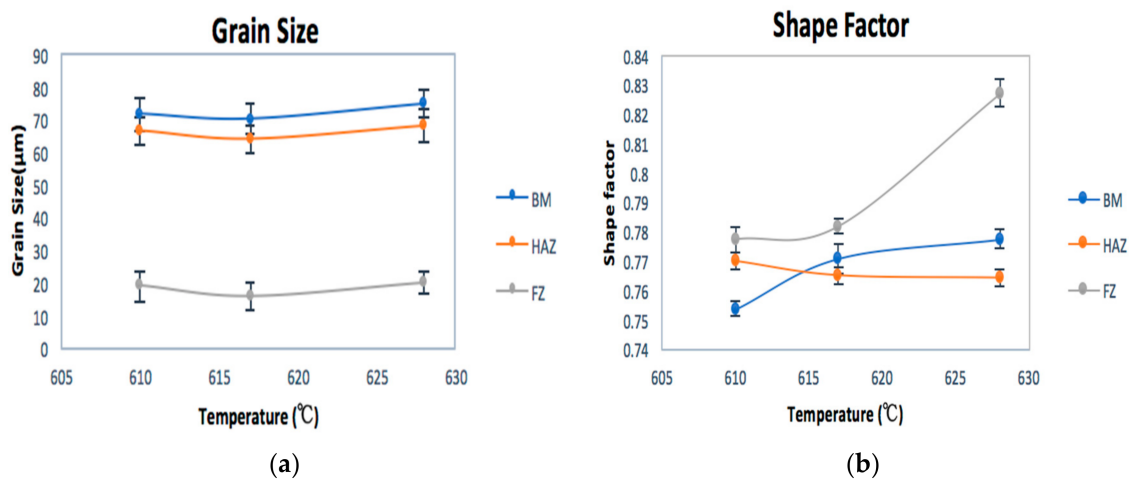


Figure 9. (a) Graph of grain size against temperature, (b) Plot of shape factor as a function of the three temperatures used, 610, 617, and 628 °C for Al 7075 alloy EB welded plates after heat treatment.

3.4. Vickers Hardness Test

Results of the Vickers hardness test performed on the EB welded plates of the thixoformed 7075 aluminium alloy are summarised in Figure 10. As can be observed, the graph shows a relatively symmetric shape, and the hardness number in the BM of two plates is roughly the same, since these regions belong to the parent material with similar properties and fabrication method, either side of the weld. In addition, a rise in hardness can be observed from both plates toward the FZ. As already mentioned, evaporation of zinc was observed after welding in the FZ, however, this amount was not considerable (0.307 wt % Zn depletion based on numerical values in Table 2) and can be eliminated, so it did not cause hardness reduction in this region. Moreover, based on the results of the EDX point analysis presented before, the weight percent of Mg and Cu increased in the FZ as compared to the BM as a result of rapid cooling that occurred after the welding process. Therefore, unlike the results provided by several researchers about some alloys of aluminium, including 5005 and 2024 series showing a hardness reduction in the fusion zone due to the loss of strengthening elements, such as Cu and Mg in this area [14,18], herein the hardness increment can be attributed to the surplus amount of these strengthening elements in the FZ, supported by researchers that have reported the hardness increase that is obtained in the FZ by using appropriate filler wire during the welding process to compensate for the evaporation of elements [9].

Figure 11 illustrates Vickers hardness over distance from the weld centre after heat treatment at 610, 617 and 628 °C. The overall behaviour of the three graphs is similar, demonstrating a peak in the FZ, and as the distance from the weld centre increases, a drop in the hardness can be observed, implying property improvement in the FZ. In comparison with the graph of the EB welded plate before heat treatment in the FZ, a rise in hardness can be seen after heat treatment at the three temperatures, with hardness increasing from 144 HV before to 156, 184, and 203 HV after heat treatment at 628, 610, and 617 °C, respectively, showing a maximum at 617 °C. After heat treatment, grain growth has occurred in the FZ of the material, and, hence, a drop in hardness was expected due to grain coarsening. However, the hardness increase can be attributed to the refined grain size, as well as chemical changes in the FZ after heat treatment as different diffusion coefficients of the critical elements in the semi-solid state locally can explain the movement of atoms from the Al-lattice at these high temperatures. In addition, the hardness number at the edges of both heat-treated plates is approximately 125 HV, which is roughly the same as that in the parent material before heat treatment. It can be concluded that although heat treatment improved the hardness in the FZ, it did not change the properties of the base metal.

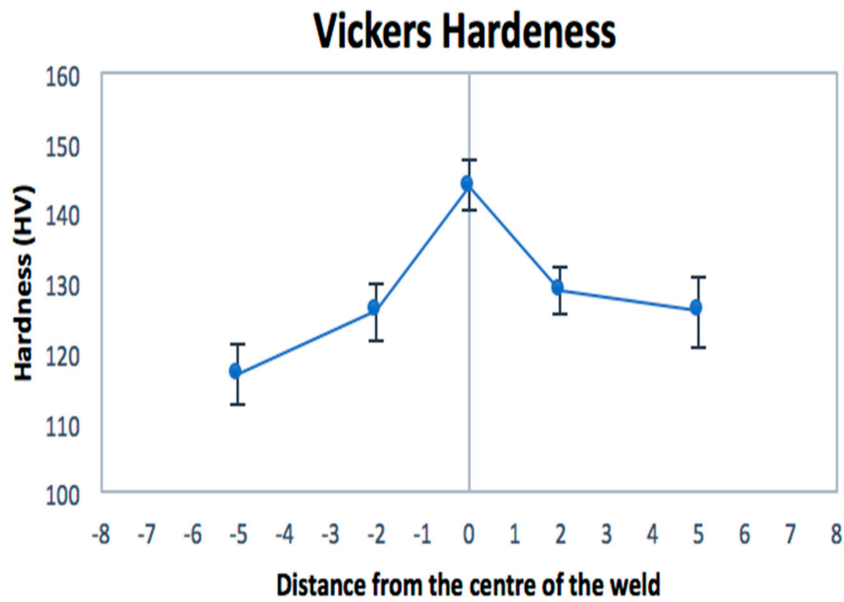


Figure 10. Graph of hardness versus position from the weld centre for Al 7075 alloy EB welded plates.

Work done by various researchers on Laser hardening, [19] has shown that the most relevant parameter in the hardened layer depth is the scanning speed, followed by the hardened track width. Another group of researchers have given a good account of modelling such processes by modelling the Added Layers by Coaxial Laser Cladding [20].

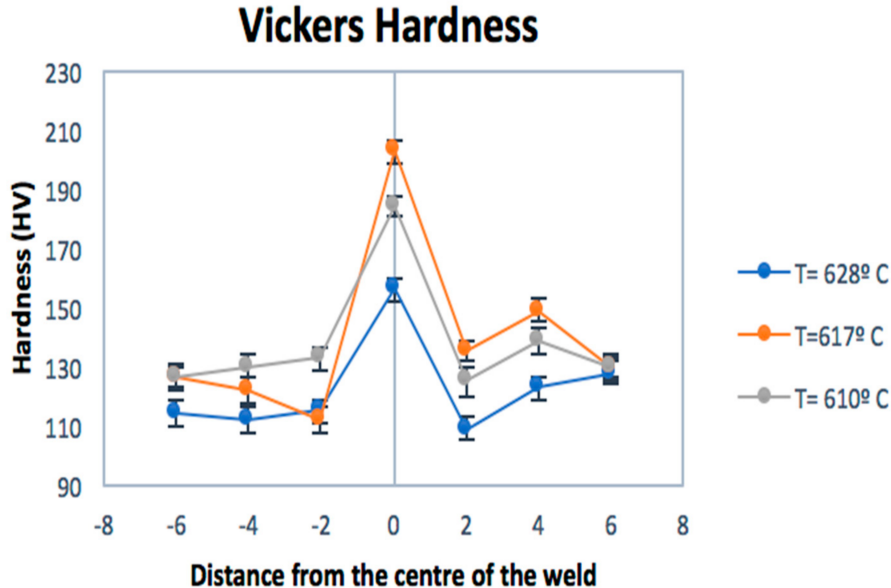


Figure 11. Graph of hardness versus position from the weld centre for Al 7075 alloy EB welded plates after heat treatment at three temperatures: 610, 617 and 628 °C.

4. Conclusions

Electron beam welding was employed on thixoformed plates of 7075 aluminium alloy, along with a post welding heat treatment in semi-solid temperature range in order to evaluate the resultant microstructures and mechanical properties in the weld area. The following conclusions were inferred from the work:

1. A fine microstructure with extremely smaller grain size than that in the parent material and HAZ was obtained in FZ of the electron beam welded plates, due to complete melting, followed by rapid cooling of the weld area.
2. Post weld heat treatment in the semi-solid range, 610, 617, and 628 °C, resulted in the growth of recrystallized grains in the fusion zone of the EB welded plates, with grains becoming more spherical in the FZ.
3. The results of EDX point analysis revealed that the weight percent of Mg and Cu increased in the FZ after electron beam welding leading to a rise in hardness in this area when compared to the BM and HAZ.
4. A further increase of hardness was obtained in FZ after post weld heat treatment in the semi-solid temperature range.

Acknowledgments: Technical staff at the University of Sheffield for their support in various analytical techniques used in this work.

Author Contributions: For research articles with several authors, a short paragraph specifying their individual contributions must be provided. The following statements should be used: Ava Azadi Chegeni and Platon Kapranos conceived and designed the experiments; Avi Azadi Chegeni performed the experiments; Avi Azadi Chegeni and Platon Kapranos analyzed the data; Avi Azadi Chegeni and Platon Kapranos wrote the paper.

Conflicts of Interest: The authors declare no conflict of interest.

References

1. Rachmat, R.S.; Takano, H.; Ikeya, N.; Kamado, S.; Kojima, Y. Application of Semi-Solid Forming to 2024 and 7075 Wrought Aluminium Billets Fabricated by EMC Process. *Mater. Sci. Forum* **2000**, *329–330*, 487–492. [[CrossRef](#)]
2. Li, J.F.; Peng, Z.W.; Li, C.X.; Jia, Z.Q.; Chen, W.J.; Zheng, Z.Q. Mechanical properties, corrosion behaviors and microstructures of 7075 aluminum alloy with various aging treatments. *Trans. Nonferrous Met. Soc. China* **2008**, *18*, 755–762. [[CrossRef](#)]
3. Williams, J.C.; Starke, E.A. Progress in structural materials for aerospace systems. *Acta Mater.* **2003**, *51*, 5775–5799. [[CrossRef](#)]
4. Isadare, A.D.; Aremo, B.; Adeoye, M.O.; Olawale, O.J.; Shittu, M.D. Effect of heat treatment on some mechanical properties of 7075 aluminum alloy. *Mater. Res.* **2013**, *16*, 190–194. [[CrossRef](#)]
5. Binesh, B.; Aghaie-Khafri, M. Phase evolution and mechanical behaviour of the semi-solid SIMA processed 7075 aluminium alloy. *Metals* **2016**, *6*, 42. [[CrossRef](#)]
6. Kapranos, P.; Ridgway, K.; Jirattiticharoen, W.; Haga, T.; Thomas, W. Friction Stir Welding (FSW) of Thixoformed and Rheocast Plates. In Proceedings of the 8th SSM Conference, Limassol, Cyprus, 21–23 September 2004.
7. Nakato, H.; Oka, M.; Itoyama, S.; Urata, M.; Kawasaki, T.; Hashiguchi, K.; Okano, S. Continuous semi-solid casting process for aluminium alloy billets. *Mater. Trans.* **2002**, *43*, 24–29. [[CrossRef](#)]
8. Chayong, S.; Atkinson, H.V.; Kapranos, P. Thixoforming 7075 aluminum alloys. *Mater. Sci. Eng. A* **2005**, *390*, 3–12. [[CrossRef](#)]
9. Cam, G.; Ipekoglu, G. Recent developments in joining of aluminium alloys. *Int. J. Adv. Manuf. Technol.* **2017**, *91*, 1851–1866. [[CrossRef](#)]
10. Cam, G.; Mistikoglu, S. Recent Developments in Friction Stir Welding of Al-alloys. *J. Mater. Eng. Perform.* **2014**, *23*, 1936–1953. [[CrossRef](#)]
11. Weglowski, M.S.; Blacha, S.; Phillips, A. Electron beam welding-techniques and trends-Review. In Proceedings of the 9th Symposium on Vacuum Based Science and Technology, Kolobrzeg, Poland, 17–19 November 2015; Programon-Elsevier Science Ltd.
12. Cam, G.; Kocak, M. Microstructural and mechanical characterization of electron beam welded Al-alloy 7020. *J. Mater. Sci.* **2007**, *42*, 7154–7161. [[CrossRef](#)]
13. Ning, Y.; Yao, Z.; Gua, H.; Fu, M.W. Hot deformation behaviour and hot working characteristic of Nickel-base electron beam weldments. *J. Alloys Compd.* **2014**, *584*, 402–494. [[CrossRef](#)]
14. Cam, G.; Ventzke, V.; Dos Santos, J.F.; Kocak, M.; Jennequin, G.; Gonthier-Maurin, P. Characterisation of electron beam welded aluminium alloys. *Sci. Technol. Weld. Join.* **2013**, *4*, 317–323. [[CrossRef](#)]

15. Brungraber, R.J.; Nelson, F.G. Effect of welding variables on aluminum-alloy weldments. *Weld. J.* **1973**, *52*, 97S–103S.
16. Olshanaskaya, T.V.; Salomatova, E.S.; Belenkiy, V.Y.; Trushnikov, D.N.; Permyakov, G.L. Electron Beam welding of Aluminium alloy AlMg6 with a Dynamically Positioned Electron Beam. *Int. J. Adv. Manuf. Technol.* **2017**, *89*, 3439–3450. [[CrossRef](#)]
17. Chen, S.C.; Huang, J.C. Comparison of post-Weld Microstructures and mechanical Properties of Electron- and Laser-Beam Welded 8090 Al-Li Alloy Plates. *Mater. Trans.* **1999**, *40*, 1069–1078. [[CrossRef](#)]
18. Pakdil, M.; Cam, G.; Kocak, M.; Erim, S. Microstructural and mechanical characterization of laser beam welded AA 6056 Al-alloy. *Mater. Sci. Eng. A* **2011**, *528*, 7350–7356. [[CrossRef](#)]
19. Martínez, S.; Lamikiz, A.; Ukara, E.; Calleja, A.; Arrizubieta, J.A.; Lopez de Lacalle, L.N. Analysis of the regimes in the scanner-based laser hardening process. *Opt. Lasers Eng.* **2017**, *90*, 72–80. [[CrossRef](#)]
20. Taberero, I.; Lamikiz, A.; Martínez, S.; Ukar, E.; López de Lacalle, L.N. Geometric Modelling of Added Layers by Coaxial Laser Cladding. *Phys. Procedia* **2012**, *39*, 913–920. [[CrossRef](#)]



© 2017 by the authors. Licensee MDPI, Basel, Switzerland. This article is an open access article distributed under the terms and conditions of the Creative Commons Attribution (CC BY) license (<http://creativecommons.org/licenses/by/4.0/>).